# The influence of SACX0307-ZnO nano-composite solder alloys on the optical and thermal properties of power LEDs


## Abstract

### Purpose

This paper aims to present the results of investigations that show the influence of ZnO composite soldering paste on the optical and thermal parameters of power LEDs.

### Design/methodology/approach

ZnO nano-composite solder alloys were produced via the ball milling process from the solder paste SACX0307 (Sn99Ag0.3Cu0.7) and 1.0 wt.% of ZnO nanoparticle reinforcements with different primary particle sizes (200 nm, 100 nm, and 50 nm). Power LEDs were soldered onto a metal core printed circuit board (MCPCB). A self-designed LED test system was used to measure the thermal and optical characteristics of the LEDs.

### Findings

The influence of the soldering paste on the thermal and optical parameters of LEDs was observed. In all solder alloys, ZnO ceramic reinforcement increased the thermal parameters of LEDs and decreases their luminous efficiency. Thermal resistance values were10% higher, and junction temperature change over ambient temperature was 20% higher for the samples soldered with composite solder pastes, as compared to the reference sample. At the same time, luminous efficiency dropped by 32%.

### Originality/value

The results prove that ZnO ceramic reinforcement of solder paste influences the thermal properties of solder joints. As it was proven, the quality of the solder joints influences the whole assembly.



**Keywords:** SACX composite alloys, ZnO, power LEDs, transient thermal impedance, thermal resistance, optical efficiency, luminous efficiency


## Introduction

Assembling of circuits is still a challenging task. Considering the growing requirements regarding the reliability and quality of circuits, the typical joining methods need to be improved. Recently, low silver content alloys have been used on the market (e.g. SACX 0307), but this alloy shows lower thermo-mechanical reliability of the solder joints as compared to typical SAC alloys and other reliability problems like electromigration (Medgyes, et al., 2013, 2015). In order to improve the mechanical properties of the solder joints, ceramic reinforcement particles are used, which results in composite solder joints (Ani et al., 2018; Skwarek et al., 2020). The size of the reinforcement particles is usually within the submicron and nano range. The most frequently used ceramics are TiO2 and ZnO. Its most significant advantages are its

high performance in photoelectricity and good physical and chemical properties such as its high melting point (1975 °C), good thermal stability, and favorable elastic modulus (Peng et. al, 2016). Like $TiO_2$, ZnO influences the microstructure of the solder joints. The composite solder joints, with the addition of ZnO, exhibit a lower IMC (*intermetallic compound*) growth speed during isothermal aging. An improvement of around 18% in microhardness and an enhancement of around 10% in shear strength were also achieved for composite solder joints after the addition of 1 wt% ZnO (Peng et al., 2016). Peng et al. observed an improvement in yield strength (YS) and ultimate tensile strength (UTS) after the addition of ZnO nanoparticles (Peng et al., 2016). Unfortunately, ZnO tends to agglomerate (especially when micrometer size); therefore, it performs worse in the soldering paste. Moreover, studies have shown that only 12% of initially doped ZnO remains in the solder alloy (Peng et al., 2016). The rest is expelled with the flux during the soldering process.

Grain-size refinement is a well-known strengthening structure mechanism in metals and alloys. The addition of ZnO nanoparticles to SAC305 alloy results in a substantial decrease in β-Sn grain size from 75μm to even several μm. The reason is that during solidification ZnO nanoparticles promote a high nucleation density of the second phase in the eutectic colony. This shows that ZnO nanoparticles have a great ability to control grain growth during solid-state cooling (El-Daly et al., 2014). The most likely explanation for the refinement of the solder microstructure (by the presence of the nano-sized ZnO particles) is surface adsorption theory. The ZnO nanoparticles incorporated into the solder cannot wet the β-Sn matrix during the solidification process. They do not form IMCs in the solder matrix, and they are non-coarsening and non-reacting. The refinement of the microstructure is caused by the high surface free energy on the solidified grain surfaces through the matrix, which adsorbs the ZnO nanoparticles during the solidification process (El-Rehim et al., 2019). Basically, ceramic particles serve as an obstacle to grain growth and retard the dislocation motion, finally resulting in the strengthening of solder joints. But the presence of ceramic reinforcement (like e.g. ZnO) leads to changes in the microstructure of the solder joint (decreases the thickness of the IMC layer and decreases of β-Sn grains size). This altered microstructure influences the other parameters of the mounted structures (Krammer et al., 2015, Garami and Krammer, 2015).

The effect of ceramic reinforcement on the mechanical parameters of the solder joint has been widely researched. However, the influence of ceramic reinforcement on the thermal properties of the solder joints and the whole is still not described enough. Because the incorporation of ceramic particles into the solder joint changes the thermal and electrical parameters of the connection, it is assumed that this will influence the thermal and optical parameters of the assembly of light-emitting diodes (LEDs) as well (Biber, 2008), (Chang, et al., 2012). Light-emitting diodes (LEDs) are commonly used in automotive and lighting techniques (Weir, 2012). The luminous flux emitted strongly depends on the temperature (Schubert, 2008), (Farkas, et al., 2018), (Poppe, 2015). According to Lasance and Poppe (2014) the internal temperature of power LEDs is the sum of the ambient temperature $T_a$ and the temperature increase above ambient temperature. The value of this increase depends on the power dissipated in the device and on the efficiency of the removal heat generated (Poppe and Lasance, 2009). This efficiency is characterized by thermal parameters as transient thermal impedance $Z_{th}(t)$ and thermal resistance $R_{th}$ (Górecki and Ptak, 2020). The optical and thermal parameters strongly depend on the properties of the solder joints (Dziurdzia et al., 2019). It has also been proven that

soldering the elements with a large thermal pad ( LEDs) encourages other reliability problems (Dziurdzia and Mikołajek 2017, Dziurdzia et al. 2018).

In this paper, the measurements results of the thermal and optical parameters of power LEDs soldered with composite solder alloys and reinforced with ZnO nanoparticles are presented and discussed. Different primary particle sizes of ZnO were used. The results were compared with measurements performed for the classic alloy SACX0307.

## 2. Materials and methods

*2. 1. Samples preparation*

Nano-composite solder alloys were produced via the ball milling process from the solder paste SACX0307 (Sn99Ag0.3Cu0.7) and 1.0 wt.% of ZnO reinforcement nanoparticles with different sizes. The primary particle sizes of the ceramics were 50 nm, 100nm, and 200nm. The mixing process was carried out for 10 min at 300 rpm using a planetary ball mill to ensure that the nanoparticles were distributed in the solder paste homogeneously. The scheme is shown in Fig. 1. The reference samples are referred to as SACX0307, and the nano-composite samples are referred to as SACX0307-ZnO (50, 100, and 200nm).

MCPCBs (Metal Core Printed Circuit Board) with 2.4 mm thickness were used as substrates. The contact surfaces were prepared from a 60 μm thick Cu layer with galvanic Ni/Au (2.5 μm/ 0.25 μm) surface finishing. Fig. 2 shows the LED test structure on the MCPCB. The power LEDs were soldered onto the substrates in an SMT 460C convection reflow oven. The soldering profile was: pre-heating for 200s in temperature 160-180°C, reflowing for 40s in temperature 213-247°C, and cooling for 50s in temperature 247-150°C. The soldering profile is shown in Fig. 3. Three samples of each type were fabricated.

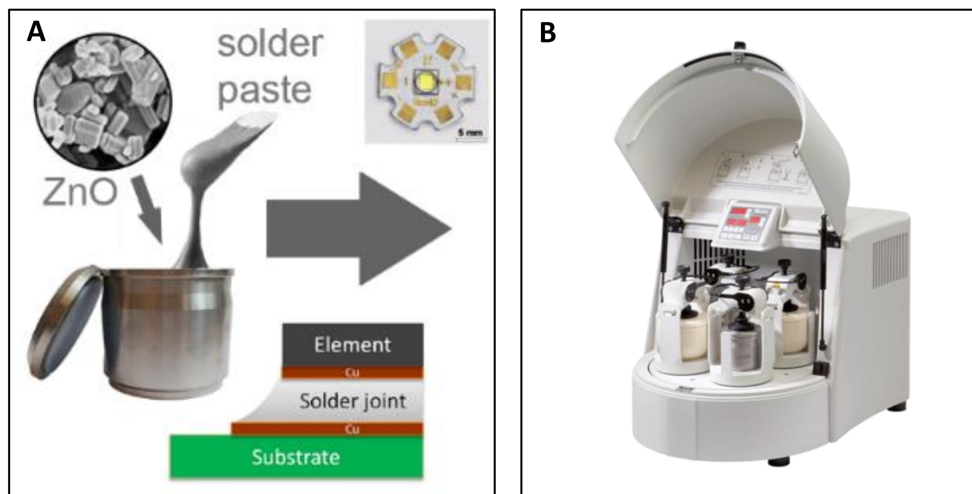


Fig. 1 A-composite solder paste preparation, B- planetary ball mill used to prepare it.

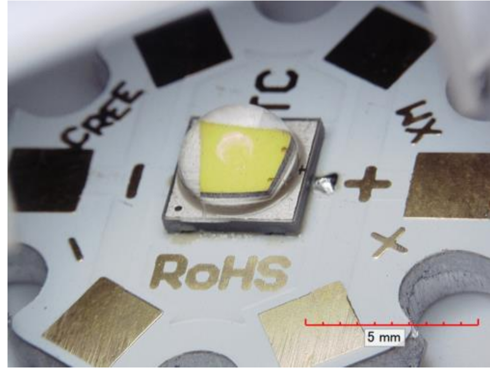


Fig. 2. LED tested structure mounted on MCPCB (Skwarek et al., 2020)

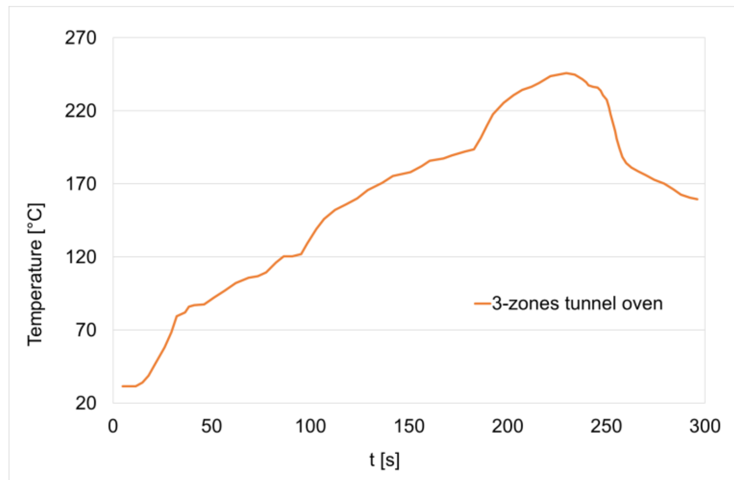


Fig. 3 Soldering profile.

*2.2. Measurement method and set-up*

In order to measure the thermal and optical parameters of power LEDs, the measuring-set-up was developed, as is shown in Fig.4. The set-up allows the transient thermal impedance $Z_{th}(t)$ of the LEDs, the illuminance E, and the power density $E_e$ of the emitted light to be measured.

The device being tested (DUT) is placed on the heat exchanger, which is part of the forced liquid cooling system (Alphacool, 2020). The heat exchanger is placed at the bottom of a light-tight and thermal chamber. The luxmeter and radiometer probes are located at the top of the chamber. DUT is supplied from the voltage source $E_H$ with the current $I_H$ regulated by the $R_H$ resistor. The current flows only if switch S is closed. In turn, the measurement current $I_M$ flows from the voltage source $E_M$ through the $R_M$ resistor.

Transient thermal impedance $Z_{th}(t)$ is measured using the indirect electrical method described in the work of Górecki and Ptak (Górecki and Ptak, 2020). In these methods, the values of the device junction temperature occurring in the definition of $Z_{th}(t)$ are measured with the aid of the thermo-sensitive parameter. This parameter is known for being dependent on temperature. This method uses a voltage drop $V_D$ on DUT at the fixed value of the forward current $I_M$ as a thermo-sensitive parameter.

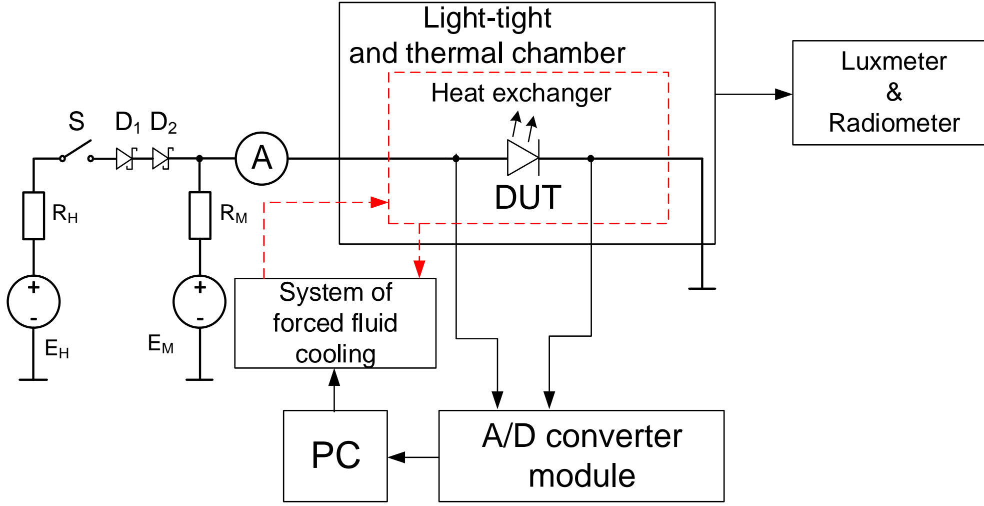


Fig. 3. Diagram of the measurement set-up

Measurements of transient thermal impedance are performed in 4 steps. First, the thermometric characteristic $V_D(T)$ at the current $I_M$ is measured at opened switch S. The slope of this characteristic amounts to $\alpha_T$. In the second step, the switch S is closed, and DUT is heated by the current $I_H$, which flow causing an increase in its internal temperature. At the steady-state, $I_H$ current, $V_H$ voltage illuminance E, and optical power density $E_e$ are registered. In the third step, from moment t = 0 (switching off the switch S) cooling starts, and the A/D converter measures the waveform of voltage $V_D$ at current $I_M$ until the steady-state is reached. The waveform of transient thermal impedance is calculated using the following formula (Górecki and Ptak, 2020):

$$Z_{th}(t) = \frac{V_D(t) - V_D(t=0)}{\alpha_T \cdot (V_H \cdot I_H - P_{opt})} \tag{1}$$

where $P_{opt}$ is optical power. Thermal resistance $R_{th}$ is the value of $Z_{th}(t)$ at the steady-state.

Optical power is measured using the method described in the paper by Górecki and Ptak (Górecki and Ptak, 2018) on the basis of the power density of emitted light $E_e$ measured at distance $r$ between the radiometer probe and surface of DUT in the axis of DUT.

This method also uses the spatial radiation patterns of the DUT given by the manufacturer. The relative surface power density of the optical radiation $\alpha_{opt}$, and the emission angle $\alpha_{max}$ at $E_e$ = 0 are determined using this characteristic. The value of $P_{opt}$ is calculated using the following formula:

$$P_{opt} = 2 \cdot E_e \cdot \pi \cdot r^2 \cdot (1 - \cos\alpha_{max}) \cdot \left(a \cdot \alpha_{max}^2 / 3 + 2 \cdot c\right) \tag{2}$$

where $a$ and $c$ are coefficients of square function approximating spatial radiation patterns.

The luminous flux $\Phi_V$ is calculated using the following formula:

$$\Phi_V = 2 \cdot E \cdot \pi \cdot r^2 \cdot (1 - \cos\alpha_{max}) \cdot \left(a \cdot \alpha_{max}^2 / 3 + 2 \cdot c\right) \tag{3}$$

where E is illuminance measured at distance r between the luxmeter probe and the surface of DUT in the axis of DUT.

In order to describe the efficiency of the conversion of electrical energy into light in power LEDs two parameters are used. Optical efficiency $\eta_{opt}$ is defined as the quotient of the optical power $P_{opt}$ and electrical power consumed by LED. Parameter $\eta_{opt}$ is given by the following equation:

$$\eta_{opt} = \frac{P_{opt}}{V_H \cdot I_H} \tag{4}$$

In turn, luminous efficiency $\eta_F$ is defined as the quotient of the value of the emitted luminous flux of the emitted light and electrical power consumed by an LED according to the following formula:

$$\eta_F = \frac{\Phi_V}{V_H \cdot I_H} \tag{5}$$

Formulas presented in equations 2-5 allow for the calculations of optical power, luminous flux, optical efficiency, and luminous efficiency on the basis of emitted light power density ($E_e$), illuminance ($E$) in the distance from the surface of DUT ($r$), diode voltage ($V_H$) at current ($I_H$). Measurements of all the quantities mentioned above are performed simultaneously at the thermally steady state. It allows for the characterization of LED thermal and optical parameters and conclusions about solder joint influence on these assemblies.

**3. Results and discussion**

Using the measurement method described above, the thermal and optical parameters of the samples were measured. While the measurements were being taken the distance $r$ was equal to 255mm and the emission angle for the LED was $\alpha_{max} = 85°$. To ensure the measurements were highly sensitive and to limit the margin of error (Górecki and Górecki, 2015), the forward current $I_H$ was increased to 5A. It exceeded the admissible catalog value, equal to 3A, but due to the use of the fluidic cooling system, it was possible to limit the value of the internal temperature to 110°C. This value is considerably lower than the admissible catalog value of the junction temperature $T_{jmax} = 150°C$ (XML2, 2020).

In the first step, the waveform of transient thermal impedance $Z_{th}(t)$ was measured, and the values of the following parameters at the thermally steady state were determined: thermal resistance $R_{th}$, luminous flux $\Phi_V$, optical power $P_{opt}$, optical efficiency $\eta_{opt}$, and luminous efficiency $\eta_F$. Figure 5 shows the transient thermal impedance waveform of the samples soldered with ZnO (1 wt.%) composite pastes and the reference sample (SACX0307). For all samples, a thermally steady state is observed after 1000 s (Fig. 5A). However, visible differences between $Z_{th}(t)$ waveforms were observed at the steady-state. For all samples soldered with composite pastes, the calculated value of $R_{th}$ (Fig. 5B) is higher by as much as 10% in comparison to the reference samples. The ZnO primary particle sizes (50, 100 or 200nm) do not influence the thermal resistance of the samples (the differences not exceeding 1%).

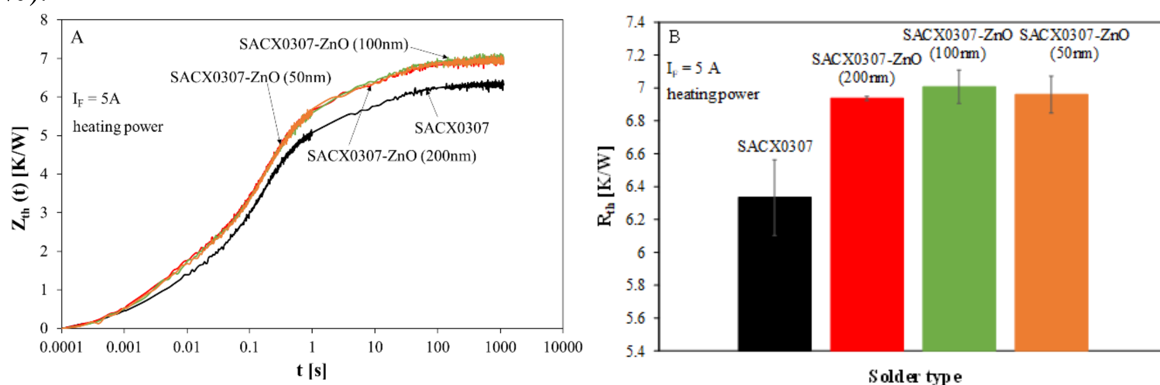


Fig. 5 A – Transient thermal impedance ($Z_{th}(t)$) waveforms, and B- thermal resistance ($R_{th}$) for the LEDs soldered with different composite pastes.

Fig. 6 illustrates the influence of the soldering paste on junction temperature change over ambient temperature ($\Delta T_j$). The $\Delta T_j$ waveforms during cooling are shown in Fig. 6A. Fig. 6B presents $\Delta T_j$ values before cooling at the steady-state. At forward current $I_H = 5A$, the junction temperature changes $\Delta T_j$ are the smallest for the reference solder alloy (almost 20 °C lower than for composite solder alloys). The highest junction temperature was observed for the composite solder alloy SACX0307 (100nm). This shows that composite solder pastes increase the junction temperature of LEDs significantly. Such a difference of $\Delta T_j$ can cause up to a fourfold decrease in the lifetime of the device being tested (Narendran and Gu, 2005).

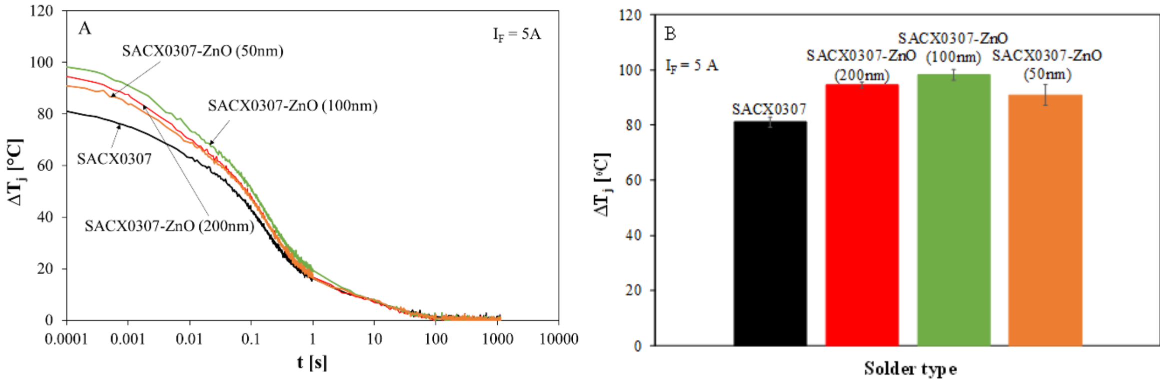


Fig. 6. A – Waveforms of junction temperature change over ambient temperature ($\Delta T_j$) while cooling, B - $\Delta T_j$ values before cooling at the steady-state for the LEDs soldered with different composite pastes.

Fig. 7 presents the optical efficiency of all samples (Fig. 7A) and averaged values of this parameter (Fig. 7B).

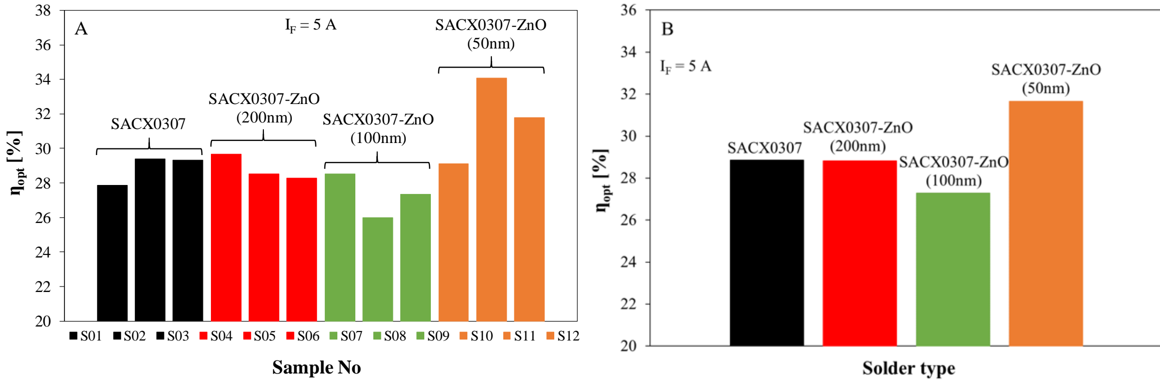


Fig. 7. The optical efficiency of LEDs soldered with different composite solder pastes. A-single measurements, B-average value.

It seems that the composition of solder alloys slightly influences optical efficiency (Fig. 7A). For the reference sample, optical efficiency reaches 29%. SACX0307-ZnO (200nm) and SACX0307-ZnO (100nm) have similar values (around 28%). The samples soldered with SACX0307-ZnO (50nm) show an increase of this parameter to 32%; however, standard deviation is high.

Fig. 8 illustrates the values of the luminous efficiency of the LEDs (Fig. 8A) and the averaged values of this parameter (Fig. 8B).

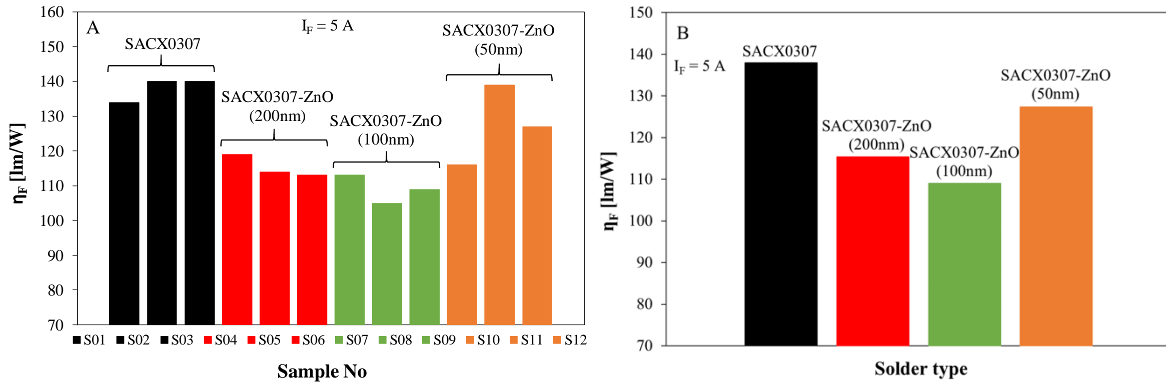


Fig. 8. Luminous efficiency of LEDs soldered with different composite solder pastes. A- single measurements, B- average values.

The luminous efficiency value decreased in the reinforced nano-composite solder joints compared to the reference samples (Fig. 8A). The highest value was observed for the reference samples (SACX0307). The differences between the reference samples and nano-composite ones reached 29 lm/W (Fig. 8B), which corresponds to 20% drop from the reference samples.

The results presented in Figs. 5-8 show that the use of solder alloys with ZnO reinforcement causes an increase in thermal resistance and a decrease in optical efficiency and luminous efficiency. At a high value of diode forward current, an increase in $R_{th}$ can cause a visible increase in the internal temperature of the device and an up to a fourfold decrease in its lifetime. It is worth noticing that when the internal temperature of the device is higher, the optical efficiency has its highest value for the solder alloy with ZnO with a primary particle size of 50 nm. This means that from the point of view of the LED optical parameters optimization this solder alloy is the most profitable.

Compared to the results of 1wt% $TiO_2$ addition (Skwarek et al., 2020), 1wt % addition of ZnO into the solder paste showed different results. Lower thermal and optical parameters of LEDs were probably related to the lower wettability and higher void formation in the case of the ZnO composite solder joint. Composite solder pastes with the addition of ZnO are much more prone to void formation due to the lower wettability of the ZnO nano-composite solder pastes. This is related to the fact that ZnO is an amphoteric oxide, insoluble in water but soluble in most acids. One of the components of the solder paste is acid-based flux. The chemical reaction between ZnO and acid might change the surface tension of the melted nano-composite solder alloy, resulting in poor wetting.

The other reason of the changes in thermal and optical parameters of LEDs could be the modification of solder joint microstructure. As it was proven before, the addition of ZnO changes the grains size in solder bulk and influences the IMC (*intermetallic compounds*) presence as well (Skwarek et al., 2021). Therefore the microstructures of the composite solder joints and the reference solder joints have been compared by scanning electron microscopy and energy-dispersive X-ray spectroscopy (EDX) (Fig. 9). Although in all cases, the typical IMC structures are visible i. e. IMC layer on Cu/Sn interphase and spaced IMCs ($Cu_6Sn_5$ and $Ag_3Sn$), the samples differ from each other. Sn grains in the composite solder joints were much finer than in the reference sample. Ceramic particles effectively block grain growth. Also, $Cu_6Sn_5$ and $Ag_3Sn$ spacing were lower. The $Ag_3Sn$ IMCs are incorporated at the grain boundaries of the Sn matrix as it was described earlier by Yahaya et al., 2020, so the Sn grain boundaries can

be located according to the $Ag_3Sn$ network in the solder bulk. The grain boundaries are marked by red dashed lines in Fig. 9. During the solidification, the ZnO particles resulted in a high nucleation density in the second phase of the eutectic colony. The addition of ZnO nano-particles resulted in considerable refinement of the Sn grains in each case, from ~20–30 $\mu m^2$ to ~2–4 $\mu m^2$. This shows that ZnO nanoparticles have an increased ability to limit grain growth during solid-state cooling (Skwarek et al., 2021). The Sn grain refinement did not depend on the ZnO particle sizes. According to the literature, modifications in the solder bulk microstructure lead to the changes of the Sn layer thermal conductivity (Noh et al., 2006) and, finally optical and thermal parameters of LED assemblies (Skwarek et al., 2020).

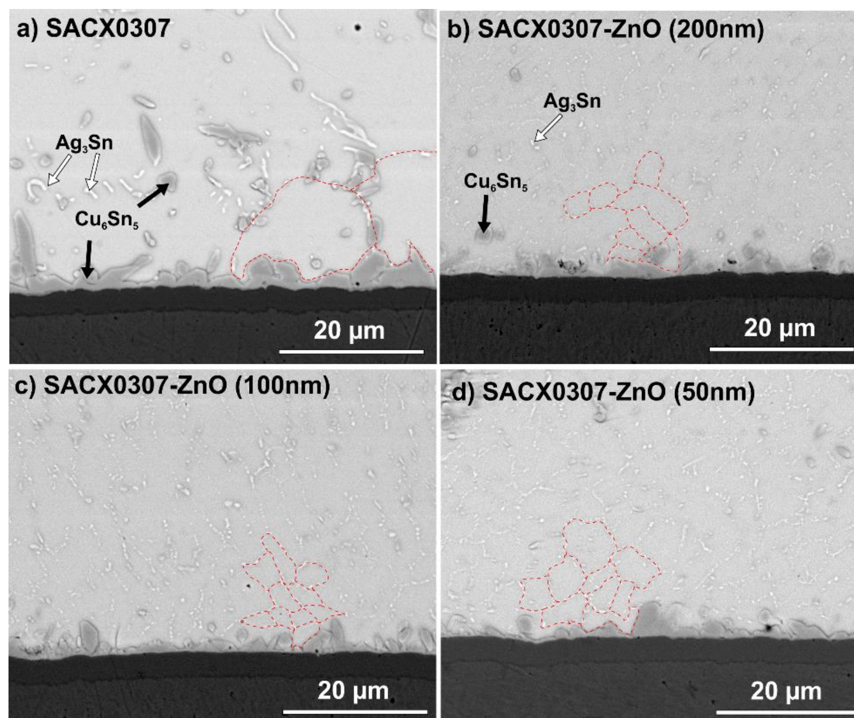


Fig. 9 SEM micrograph of the microstructure in the different solder joints: (**a**) SACX0307; (**b**) SACX0307-ZnO-(200 nm); (**c**) SACX0307-ZnO-(100 nm); (**d**) SACX0307-ZnO-(50 nm).

**Summary**

Three different SACX0307-ZnO composite solder alloys were fabricated with different primary particle sizes: 50, 100, and 200 nm. The reference sample was SACX0307. It was proven that ZnO ceramic reinforcement in all solder alloy increases the thermal parameters of LEDs and decreases luminous efficiency. Thermal resistance $R_{th}$ values were 10% higher and $\Delta T_j$ 20% higher for the samples soldered with composite solder pastes, as compared to the reference sample. Simultaneously $\eta_F$ dropped by 32%.

The $\eta_{opt}$ stayed on the same level for all samples i.e soldered with ZnO composite pastes and reference paste (SACX0307), except SACX0307-ZnO (50nm).

The results showed that ZnO addition to the solder paste at a level of 1wt % did not improve the thermal and optical parameters of LED assemblies as compared e.g. to $TiO_2$. It is assumed that the lowest ZnO content in the solder paste could give much better results. These findings

are important for the further development of composite solder alloys as well as power LED light sources.

## ACKNOWLEDGEMENTS

This study was partially supported by the Ministry of Science and Higher Education –Poland (MNiSW) as part of project No. 006/RID/2018/19 financed by the program "Regionalna Inicjatywa Doskonałości 2019-2022", the amount provided being 11 870 000 PLN and by the National Research Development and Innovation Office—Hungary (NKFIH) as part of Project Number FK 127970.

**References**

Alphacool Comapny site. Availaible online: https://www.alphacool.com/, (accessed 22 Jan 2020).

Ani, F.C., Jalar, A., Saad, A.A., Khor, C.Y., Ismail, R., Bachok, Z., Abas, M.A. and Othman, N.K. (2018), "SAC–xTiO2 nano-reinforced lead-free solder joint characterizations in ultra-fine package assembly", *Soldering & Surface Mount Technology* Vol. 30, No. 1, pp. 1-13.

Biber, C. (2008), "LED Light emission as a function of thermal conditions", *Proceedings of the 24th IEEE Semiconductor Thermal Measurement and Management Symposium*, San Jose, CA, USA, pp. 180-184.

Chang, M.H., Das, D., Varde, P.V. and Pecht, M. (2012), "Light emitting diodes reliability review", *Microelectronics Reliability*, Vol. 52, pp. 762-782.

Dziurdzia, B., Górecki, K. and Ptak, P. (2019), "Influence of a soldering process on thermal parameters of large power LED modules", *IEEE Transactions on Components, Packaging and Manufacturing Technology*, Vol. 9, No. 11, pp. 2160-2167.

Dziurdzia, B. and Mikołajek, J. (2017), "X-ray inspection and Six-Sigma in analysis of LED thermal pad coverage", *Soldering & Surface Mount Technology*, Vol. 29, No. 1, pp. 28-33.

Dziurdzia, B., Sobolewski, M. and Mikolajek, J. (2018), "Convection vs vapour phase reflow in LED and BGA assembly", *Soldering & Surface Mount Technology*, Vol. 30, No. 2, pp. 87-99.

El-Daly A.A., Elmosalami T.A, Desoky W.M., El-Shaarawy M.G., Abdraboh A.M. (2014), "Tensile deformation behavior and melting property of nano-sized ZnO particles reinforced Sn–3.0 Ag–0.5 Cu lead-free solder" Materials Science and Engineering A, Vol. 618, pp. 389–397.

El-Rehim A.F.A., Zahran H.Y., Yassin A.M. (2019), "Microstructure evolution and tensile creep behavior of Sn–0.7 Cu lead-free solder reinforced with ZnO nanoparticles", *Journal of Materials Science: Materials in Electronics*, Vol. 30, pp. 2213–2223.

Farkas, G., Poppe, A., Gaal, L., Hantos, G., Barenyi, Cs. and Rencz, M. (2018), "Structural analysis and modelling of packaged light emitting devices by thermal transient measurements at multiple boundaries". 24th International Workshop on Thermal Investigations of ICs and Systems Therminic 2018, Stockholm.

Garami, T. and Krammer, O., (2015), "Quantitative analyses of Ag3Sn intermetallic compound formation in SnAgCu solder alloys", *Journal of Materials Science: Materials in* Electronics, Vol. 26, No. 11, pp. 8540–8547.

Górecki, K. and Górecki, P. (2015), "The Analysis of Accuracy of Selected Methods of Measuring the Thermal Resistance of IGBTs", *Metrology and Measurement Systems*, Vol. 22, No. 3, pp. 455-464.

Górecki, K. and Ptak, P. (2018), "New dynamic electro-thermo-optical model of power LEDs". Microelectronics Reliability, Vol. 91, pp. 1-7.

Górecki, K. and Ptak, P. (2020), "New method of measurements transient thermal impedance and radial power of power LEDs", *IEEE Transactions on Instrumentation and Measurement*, Vol. 69, No. 1, pp. 212-220.

Krammer, O., Garami, T., Horváth, B., Hurtony, T., Medgyes, B. and Jakab, L. (2015), "Investigating the thermomechanical properties and intermetallic layer formation of Bi micro-alloyed low-Ag content solders", *Journal of Alloys and Compounds*, Vol. 634, pp. 156-162.

Lasance, C.J.M. and Poppe, A. (2014), "*Thermal management for LED applications*", Springer Science+Business Media, New York, USA.

Medgyes, B., Horváth, B., Illés, B., Shinohara, T., Tahara, A., Harsányi, G. and Krammer, O., (2015), "Microstructure and Elemental Composition of Electrochemically formed Dendrites in case of Lead-free Micro-alloyed low Ag Solder Alloys used in Electronics", Corrosion Science, Vol. 92, pp. 43-47.

Medgyes, B., Illés, B. and Harsányi, G., (2013) "Electrochemical Migration of Micro-alloyed Low Ag Solders in

NaCl Solution", Periodica Polytechnica - Electrical Engineering, Vol. 57, No. 2, pp. 49-55.

Narendran N., Gu Y. (2005), "Life of LED-based white light sources", *Journal of Display Technology*, Vol. 1, No. 1, pp. 167-171.

Noh, B.I., Koo J.M., Kim J. W., Kim D.G., Nam J. D., Joo J., Jung S.B. (2006), "Effects of number of reflows on the mechanical and electrical properties of BGA package", *Intermetallics*, Vol. 14/10–11, pp. 1375-1378

Peng H., Chen G., Mo L., Chan Y. C., Wu F., Liu H. (2016), "An investigation on the ZnO retained ratio, microstructural evolution, and mechanical properties of ZnO doped Sn3. 0Ag0. 5Cu composite solder joints", *Journal of Materials Science: Materials in Electronics,* Vol. 27, pp. 9083–9093.

Poppe, A. (2015), "Multi-domain compact modeling of LEDs: An overview of models and experimental data", *Microelectronic Journal,* Vol. 46, pp. 1138-1151.

Poppe, A. and Lasance, C.J.M. (2009), "On the standardization of thermal characterization of LEDs", *Proceedings of the 25th Annual IEEE Semiconductor Thermal Measurement and Management Symposium*, San Jose, CA, USA, pp. 151-158.

Schubert, E.F. (2008), *"Light emitting diodes"*, 2nd ed., Cambridge University Press, New York, USA.

Skwarek, A., Ptak, P., Górecki, K., Hurtony, T.,Illés B. (2020), "Microstructure influence of SACX0307-TiO2 composite solder joints on thermal properties of power LED assembly" *Materials*, Vol 13, No. 7, 1563.

1. Skwarek, A. Krammer, O., Hurtony, T., Ptak, P., Górecki, K., Wroński, S. , Straubinger, D., Witek, K., Illés, B. (2021), "Application of ZnO Nanoparticles in Sn99Ag0.3 Cu0.7-Based Composite Solder Alloys", Nanomaterials, 11, 1545. Yahaya, M. Z.; Nazeri, M. F. M.; Kheawhom, S.; Illés, B.; Skwarek A.; Mohamad, A. A. (2020) "Microstructural analysis of Sn-3.0Ag-0.5Cu-TiO2 composite solder alloy after selective electrochemical etching", *Materials Research Express* . Vol. 7, No. 1, 1-13.

Weir, B. (2012), "Driving the 21st Century's Lights", *IEEE Spectrum*, Vol. 49, No. 3, pp. 42-47.

XML2 LED diode datasheet. Availaible online: https://www.cree.com/led-components/media/documents/XLampXML2.pdf, (accessed 22 Jan 2020).